Int J Nanomedicine. 2012; 7: 5653–5669.

Published online 2012 Nov 13. doi: 10.2147/IJN.S34574

PMCID: PMC3501399

Mechanisms of greater cardiomyocyte functions on conductive nanoengineered composites for cardiovascular application

David A Stout,[1,2] Jennie Yoo,[2] Adriana Noemi Santiago-Miranda,[3] and Thomas J Webster[1,4]

Author information ► Copyright and License information ►

This article has been corrected. See Int J Nanomedicine. 2013 January 18; 8: 295.

This article has been cited by other articles in PMC.

Abstract

Go to:

Introduction

Cardiovascular disease is a major epidemic, both in the US and worldwide. Cardiovascular disease refers to a class of diseases that affect the heart and blood vessels of the host, and usually refers to atherosclerosis or arterial disease.[1,2] Approximately every 25 seconds, an American will have a coronary event, and approximately every minute, someone will die of one.[3] On average, every 40 seconds, someone in the US has a stroke.[3] An estimated 74,500,000 adults in the US have hypertension, with approximately 78% aware of their condition and 68% using antihypertensive medication, but only 44% of those treated have their hypertension controlled.[3] The total direct and indirect costs of cardiovascular disease and stroke in the US for 2010 were estimated at $503.2 billion.[3] In recent years, cardiovascular disease has become the leading killer of American women, surpassing breast cancer. By the time cardiovascular disease has been detected, it is usually fairly advanced, having been developing for decades.[4,5]

Cardiovascular disease is the major culprit when an individual has a myocardial infarction, also known as a heart attack. This usually occurs when a blood vessel in the heart is obstructed in the myocardium and the cardiac muscle surrounding the obstruction dies as a result of oxygen deprivation. This is very important because the myocardium is composed primarily of specialized muscle cells called cardiac myocytes or cardiomyocytes. Although cardiomyocytes comprise only approximately 25% of the total number of cells in the heart, they account for more than 90% of the total myocardium volume due to their large size.[6] Therefore, when a blood vessel in the heart is blocked by an obstruction, known as an infarct, these specialized cells die. Because cardiomyocytes are terminally differentiated cells, they are usually unable to regenerate after an infarction.[7] Instead, noncontractile fibrous cells gradually begin to replace the dead cardiomyocytes, causing a thin and rigid muscular ventricular wall.[8] The scar tissue formed

reduces contractile function of the heart, causing ventricular remodeling and ultimately leading to heart failure.[9]

Although changes in environmental exposures, reduction in tobacco use, dietary adjustments, and increased physical activity can all improve patient health, the progression of cardiovascular disease is increasing worldwide. New models to detect and treat cardiovascular disease in asymptomatic patients are needed in order to prevent the first symptoms from becoming the last as a result of death. A need for improved and safer approaches to coronary and intracranial revascularization is still required, even with the advances made over the last 10 years.

Unfortunately, no single technology offers the perfect solution. To address these problems, rapid technological advances in cell biology, genomics, and proteomics combined with discoveries in material sciences and bioengineering have created a new field of medicine, known as nanomedicine, which utilizes materials and systems possessing at least one physical dimension between 1 nm and 100 nm to construct structures, devices, and systems that have novel properties.[10,11]

The advent of advanced novel nanobiomaterials with improved properties capable of being used in several biomedical applications simultaneously has transformed the field of biomedical research. Nanomaterials are among the most intensively studied materials in a wide range of applications, ranging from fuel cells[12,13] to nanopatches for the myocardium.[14,15] These nanostructured composite materials are combinations of at least two constituent materials, a matrix (host) and a reinforcement component (ie, a nanofiller).[16] It is known that the properties of materials change considerably when the size of constituents is significantly small, within the 1–100 nm size range.[17–19] Since these materials have improved physical, chemical, and mechanical properties, they are significantly versatile for a wide range of applications.

One such example is the use of a poly(lactic-co-glycolic acid) (PLGA) material with carbon nanofibers (CNF) embedded to create a “patch” for an infarcted area of the heart. Recent research has shown that when CNF is added to PLGA, cardiomyocytes (specialized heart tissue cells responsible for contraction) will adhere and proliferate better than on their counterparts which are not nano-reinforced, but the mechanism is still largely unknown.[15]

To understand further the function of cardiomyocytes and elucidate a mechanism for such interactions on exposure to PLGA:CNF materials, the purpose of this in vitro study was to alter PLGA density in an effort to shed light on material wettability, protein adsorption, conductivity, tensile strength, and cardiomyocyte function, and to clarify why cardiomyocytes favor some nanocomposites over others. The hypothesis of this study was that materials which mimic the conductivity, tensile strength, and topography of heart tissue itself will maximize cardiomyocyte function.

Go to:

Materials and methods

PLGA:CNF fabrication

PLGA:CNF composites were fabricated as described in great detail elsewhere.[15] In brief, different PLGA densities (0.1, 0.05, 0.025, and 0.0125 g/mL; 50:50 PLA:PGA wt%, Polysciences, Warrington, PA) were created by dilution in a 50 mL flask with 30 mL of tetrahydrofuran (Mallinckrodt Chemicals, St Louis, MO) and sonicated in a B3500A-DTHVWR (VWR, Watertown, MA) water bath below 30°C for 30 minutes. Next, 500 mg of CNF (99.9% by wt%, Catalytic Materials, Pittsboro, NC) with a diameter of 100 nm and different lengths from 100 to 200 microns were sonicated (Misonix Sonicator 3000, Cole-Parmer Instrument Company, Vernon Hills, IL) in a 50 mL beaker with 20 mL of chloroform (Fisher Scientific, Waltham, MA) at 20 W for 30 minutes. After obtaining the separately sonicated PLGA and CNF solutions, various PLGA:CNF weight percent ratios were developed (100:0, 75:25, 50:50, 25:75, and 0:100) by adding the appropriate amount of CNF to PLGA in 20 mL disposable scintillation vials. The CNF weight ratios were measured using a laboratory balance (Mettler Toledo AL54, Fisher Scientific). After the appropriate ratios were formed, each composite material was sonicated (Misonix Sonicator 3000) at 10 W for 20 minutes each.

For ease of experimentation, a 22 mm diameter microscope cover glass (Fisher Science circles No 1, 0.13–0.17 mm thick; size 22 mm) was coated with the aforementioned composite. Before the PLGA:CNF composite was positioned onto the glass substrate, the glass substrate was cleaned via soaking in a 70:30 (vol%) ethanol deionized solution using an advanced digital shaker (VWR) for 10 minutes. Next, the substrate was added to a 100% deionized water solution and shaken for 10 minutes.

Using a disposable pipette (Thermo Fisher Scientific, Fair Lawn, NJ), 1 mL of the appropriate PLGA:CNF composite solution was placed onto the glass substrate and placed into an oven at 42°C for 15 minutes. Each composite film was then vacuum-dried (Shel Lab Shellab, Cornelius, OR) at 20 inches of mercury gauge vacuum pressure for 48 hours to allow the tetrahydrofuran and chloroform to evaporate. All the samples and controls were sterilized using ultraviolet light for 24 hours prior to the cell experiments.

Material characterization

Scanning electron microscopy

A Hitachi 2700 scanning electron microscope (SEM) was used to characterize the surface of the PLGA:CNF samples at 5 kV utilizing an InLens system and software with magnification ranging from 1000× to 40,000×.

Atomic force microscopy

Atomic force microscopy measurements were performed using a scanning probe microscope (Asylum Research, MFP-3D Coax, Santa Barbara, CA) to create a topographical map of the surface. The analyses were performed in air and under constant applied force (noncontact mode) with a cantilever (Asylum Research) resonant frequency of about 360 kHz and a theoretical spring constant (k) of 42 $N \cdot m^{-1}$. Images were processed and analyzed using the Image Processing Data Analysis Igor Pro 6 software (WaveMetrics, Portland, OR). Material surface roughness was evaluated on topographical atomic force microscopy images and the root-mean-square data averaged as well as percent surface area increase (Eq 1) calculated over a series of six images for each sample ratio with the assistance of atomic force microscopy software (WaveMetrics, Igor Pro 6).

$$\%SA=(A_F-A_I)A_F\times 100 \quad (1)$$

where $\%SA$ is the increase in surface area (%), A_F is the final area (nm), and A_I is the initial area (nm).

Conductivity

Conductivity tests were performed to compare material characteristics of the study composite with that of the human myocardium. The electrical resistance of the dry PLGA:CNF samples was obtained by measuring sample resistance while taking geometric considerations into account. Next, 1 mL of solution was placed on a glass substrate (Fisher Science circles No 1, 0.13–0.17 mm thick; size 22 mm) and vacuum-dried for 48 hours to evaporate all of the chloroform and tetrahydrofuran. Conductivity measurements were completed using a four-point conductivity theorem (Eq 2). In brief, for a four-point probe measurement, one pair of leads was used to inject the measurement current, while a second pair of leads, in parallel with the first, was used to measure the potential drop across the device. There was no potential drop across the voltage measurement leads, so the contact resistance drop was not included, making for a more accurate system. All measurements were conducted on a four-point conductivity measurement device built inhouse and completed four times on each sample at different locations.

$$\sigma=12\pi V(1l_1+1l_3-1l_1+l_2-1l_2+l_3) \quad (2)$$

where the σ is conductivity ($S \cdot m^{-1}$), π is the number 3.14, V is voltage (v), l_1 is the length (mm) between leads 2 and 3, l_2 is the length (mm) between leads 1 and 2, and l_3 is the length between 3 and 4.

Tensile tests

Tensile tests were performed to compare material characteristics with that of the human myocardium. A negative flat test sample mold was used to create the material samples, made from Sylgard 184® (Dow Corning Inc, Midland, MI) with sample dimensions of gauge length 7.62 mm, width of gauge 3.18 mm, reduced section 9.53 mm, distance between shoulders 26.33 mm, overall length 63.55 mm, width of grip section 9.53 mm, and sample thickness 3.20 mm. Each PLGA:CNF composite ratio solution was added to the mold and vacuum-dried (Shel Lab) at 20 inches of Hg gauge vacuum pressure for 72 hours to allow for solvent evaporation. After the samples were dried and released from the mold, tensile tests were performed in a Rheometric Minimat 2000 tensile machine (Rheometric Scientific, Piscataway, NJ) at a speed of 50 mm per minute until material failure occurred in accordance with the American Society for Testing and Materials standard test method for tensile properties of plastics designation D638-10.[20]

Protein adsorption

Adsorption of proteins on the sample surfaces was accomplished using fibronectin and vitronectin. First, all the study samples were rinsed with phosphate-buffered solution (8 g NaCl, 0.2 g KCL, 1.5 g Na_2HPO_4, and 0.2 g KH_2PO_4 in 1000 mL of deionized water adjusted to a pH of 7.4) twice and placed into cell culture well plates (BD Falcon, Franklin Lakes, NJ) for sterility purposes. Two sets of similar well plates were prepared for each experiment. The first set included 1 mL of cardiomyocyte growth medium (Celprogen Inc, San Pedro, CA) supplemented with 10% fetal bovine serum (Thermo Scientific, Waltham, MA). For the second set, 1 mL of cardiomyocyte growth medium (Celprogen Inc) without fetal bovine serum was added to each well as a control. Both plates were incubated under standard conditions (at 5% CO_2 95% humidified air and 37°C) for 24 hours to allow for protein adsorption. After 24 hours, both plates were taken out, the medium was aspirated, and the samples were rinsed twice with phosphate-buffered solution. The substrate samples were then blocked with 500 µL of 2% bovine serum albumin phosphate-buffered solution for one hour. The bovine serum albumin solution was aspirated and the samples were rinsed twice with phosphate-buffered solution. Next, 500 µL of solution containing the first antibody (fibronectin, Chemicon International, Temecula, CA, 3 µg antibody in 500 µL of 1% bovine serum albumin solution) was added to each well of both plates and allowed to incubate for one hour under standard conditions of 5% CO_2, 95% humidified air, and 37°C. After one hour, the antibody solution was aspirated and rinsed with 0.05% Tween® 20 (Sigma-Aldrich, St Louis, MO) three times, each time placed on a table shaker for 5 minutes. After the last Tween 20 aspiration, 500 µL of goat antirabbit secondary antibody conjugated with a horseradish peroxidase (Bio-Rad, Hercules, CA) solution (5 µL of secondary antibody in 500 µL of 1% bovine serum albumin solution) was added to each well and incubated for one hour. The secondary antibody was then aspirated and rinsed twice with 0.05% Tween 20, each time placed on a table shaker for 5 minutes. All samples were transferred into new well plates and rinsed twice with 0.05% Tween 20, each time placed on a table shaker for 5 minutes. Next, 500 µL of 2,2′-azino-bis(3-ethylbenzothiazoline-6-sulphonic acid (Vector Laboratories Inc,

Burlinghame, CA) was added to each well and incubated at room temperature in the dark for 20 minutes. Then, 200 μL of each sample was transferred to a 96-well plate and read at 405 nm using a spectrophotometer. Readings from samples cultured in medium without fetal bovine serum were subtracted from the readings from samples cultured using medium with fetal bovine serum. This procedure was performed again with vitronectin (Chemicon) as the primary antibody. Protein OD readings were normalized to the lowest OD reading, whereas the percent surface area data were not normalized.

Due to changes in surface area between the samples of interest and this study, a unitless variable comparison equation (Eq 3) was established for the amount of protein absorbed onto the substrate surface and surface area percent increases assessed by atomic force microscopy (Eq 1). This allowed for the determination of the protein adsorption capacity for a particular sample with regard to adding CNF and without regard to the surface area of a sample.

$$\delta = \%SA\rho \tag{3}$$

where δ is the normalized protein adsorption capacity, $\%SA$ is the increase in surface area, and ρ is the normalized protein reading (OD).

Wettability

Contact angle measurements were performed using a Krüss EasyDrop system (model DSA20S) with Krüss static and dynamic contact angle software (SW4001). This was done by dropping 3 μL of distilled water onto the PLGA:CNF composites and measuring the angle between the surface and water droplet (via software). Four measurements were completed for each sample, and were performed in triplicate for each PLGA density and PLGA:CNF (wt%:wt%) composite ratio.

Material degradation and pH readings

Initial dry samples of interest were weighed (W_0) and sterilized as previously described for the degradation experiments. Next, all samples were immersed in phosphate-buffered solution and incubated under standard cell culture conditions, ie, 37°C, 5% CO_2, and 95% air. A glass substrate in phosphate-buffered solution and blank phosphate-buffered solution without substrates were used as a reference and control, respectively. After 21, 28, and 36 days, the samples were removed from phosphate-buffered solution, abundantly rinsed with deionized water to remove soluble inorganic salts, and dried in an air vacuum chamber (Shel Lab) at 20 inches of Hg gauge vacuum pressure and room temperature for 48 hours to reach a constant mass. At each time point, the samples were weighed (W_t) and percentage weight loss ($\%W_L$) with respect to incubation time was calculated (Eq 4). Percent weight loss was normalized to the amount of PLGA in the composites because CNF do not degrade.

$$\%W_L=(W_0-W_t)W_0\times100$$

(4)

where $\%W_L$ is the percent weight loss, W_O is the initial dry sample weight (mg), and W_t is the final dry sample weight at a specific time point (mg). The pH of the supernatant buffer was monitored every 3 days during the experiment using a Corning 430 pH meter (Corning Inc) to determine the acidity of the medium throughout the process.

Cardiomyocyte adhesion and proliferation

For in vitro analysis, human cardiomyocytes (Celprogen) were seeded at a density of 5.0×10^4 cells/cm^2 for the cell adhesion assay and 5.0×10^4 cells/cm^2 for the cell proliferation assay on PLGA:CNF composites in complete growth medium (Celprogen) supplemented with 10% fetal bovine serum (Thermo Scientific) and a 1% penicillin-streptomycin mixture (Fisher Scientific). Cells were seeded into 12-well human cardiomyocyte stem cell culture extracellular matrix plates (Celprogen on top of the various PLGA:CNF samples) and 22 mm microscope cover slips (Fisher Science circles No 1, 0.13–0.17 mm thick; size 22 mm) as controls. The samples were incubated for 4 hours for the cell adhesion assay and for 24, 72, and 120 hours for the cell proliferation assay under standard incubation conditions (at 5% CO_2, 95% humidified air, and 37°C, changing the medium every other day).

3-(4,5-Dimethylthiazol-2-yl)-2,5-diphenyltetrazolium bromide (MTT) CellTiter 96® nonradioactive cell proliferation assays (Promega, Madison, WI) were used to analyze the cytocompatibility properties of the composite. A fluorescence research microscope (DM5500B, Leica, Wetzlar, Germany) was used to determine cell attachment and proliferation on the PLGA:CNF samples after the prescribed time period and for comparison with the MTT results. At the end of each experiment, the samples were rinsed with phosphate-buffered solution and saturated with 10% buffer formalin acetate (Fisher Scientific) for 15 minutes. For this, the samples were again rinsed with phosphate-buffered solution twice and then dyed with 4′-6-diamidio-2-phenylindole dihydrochloride (DAPI, Molecular Probes, Eugene, OR). The samples were rinsed again and stored in phosphate-buffered solution for imaging. Samples were immediately imaged and counted, four images per sample, using a 10× objective lens.

The optical density (OD) data for the cardiomyocyte MTT assays were plotted as the mean ± standard error of the mean, and standard curve analysis for OD and total cell counts. For DAPI staining, the cardiomyocyte count was determined in at least five randomly chosen microscope fields (magnification 10×) for each sample.

Cardiomyocyte viability

To assess cell viability, the cells were seeded into 12-well plates (BD Falcon) with each sample ratio and a control glass substrate at 5.5×10^4 cells/mL, and incubated for 24, 72, and 120 hours under standard incubation conditions. A Live/Dead® viability/cytotoxicity assay kit for mammalian cells (Molecular Probes) was used to assess cell viability and morphology qualitatively. The LIVE/DEAD assay is a two-color assay simultaneously staining with green fluorescent calcein AM indicating intracellular esterase activity and red fluorescent ethidium homodimer-1 indicating loss of plasma membrane integrity. The medium was removed from each well, and the samples were washed with phosphate-buffered solution. The cells were then incubated for 30 minutes with a 500 μL solution containing 2 μM calcein AM and 4 μM ethidium homodimer-1 dissolved in phosphate-buffered solution and imaged using a fluorescence microscope (Zeiss, Axiovert 200M, Oberkochen, Germany). Samples were immediately imaged and counted, with four images per sample.

Cardiomyocyte immunofluorescence staining

To indicate cellular specificity towards normal cardiomyocyte characteristics, seeded cells were immunofluorescently stained with cardiomyocyte-specific biomarkers to demonstrate integrity of the cells, ie, connexin-43 for gap junction channels, α-SCA for cardiac myocytes, and cardiac troponin T for contractile myocytes.[21] Cardiomyocytes are interconnected by gap junction channels conducting electrical impulses and direct intercellular signaling.[22] Connexin-43 is one of the three proteins that comprise the channels. α-SCA is considered to be a specific protein found only in alpha skeletal and alpha cardiac muscle actin in cardiomyocytes.[23] Troponin T is part of the troponin complex that binds to actin in thin myofilaments, indicating the contractility of cardiomyocytes.

Cells were seeded into 12-well plates (BD Falcon) with each sample and a control glass substrate at 5×10^4cells/mL, and were incubated under standard incubation conditions for 120 hours. The medium was then removed and cell cultures were rinsed twice with phosphate-buffered solution. Cells were fixed for 15 minutes with 1–2 mL of 10% formalin acetate (Fisher Scientific), permeabilized with 0.2% Triton X-100 (Sigma-Aldrich) diluted in phosphate-buffered solution for 5 minutes, and blocked with Image-iT FX signal enhancer (Invitrogen, Carlsbad, CA) for 30 minutes at room temperature with two phosphate-buffered solution washes in between each step. Primary rabbit polyclonal anticonnexin-43, mouse monoclonal anti-α-SCA, and rabbit polyclonal anti-cardiac troponin T antibodies (Abcam, Cambridge, MA) were used at a dilution of 1:400 in phosphate-buffered solution for one hour at room temperature. Secondary Alexa Fluor 488®-conjugated goat anti-mouse IgM and anti-rabbit IgG (Invitrogen) were diluted 1:600 in phosphate-buffered solution and incubated for 60 minutes at room temperature. The nucleus was visualized using DAPI (Molecular Probes) stain in a 1:30 dilution for 15 minutes at room temperature. Samples were then mounted with ProLong Gold Antifade (Invitrogen) and imaged with a fluorescence microscope (Axiovert 200M). The images were analyzed using ImageJ

software (National Institutes of Health, Bethesda, MD) with the analysis particle tool. The images were converted to an 8-bit color scheme, then adjusted to a red/black threshold and analyzed to measure protein color concentration and compare this with the total area of the image. This was done for all stains.

Statistical analysis

Cardiomyocyte adhesion and proliferation assays were performed at least in triplicate with three repeats each, and the results were compared with a control glass surface. Analysis of variance software and a Student's *t*-test were used for determining differences between means. A P value < 0.05 was considered to be statistically significant. For correlation graphs, a curve fitting tool (MathWorks, Natick, MA) in a sigmoidal curve fit with a trust-region algorithm for nonlinear optimization was used. All experiments in this study were performed at least in triplicate, and the results were compared with a control glass surface.

Go to:

Results

Material fabrication

Representative SEM images of the as-synthesized PLGA:CNF composite surfaces can be seen in Figure 1. CNF were uniformly dispersed within the PLGA matrix and, as expected, more CNF were observed for the higher CNF ratio samples. When looking at the different PLGA densities and similar CNF ratios, uniform CNFs were again uniformly dispersed within the PLGA matrix, suggesting that the materials were properly synthesized (Figure 1).

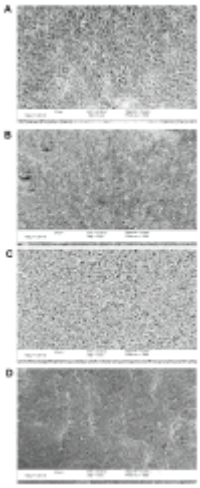

Figure 1

Scanning electron microscopic images at 5000× magnification showing distribution of CNF fibers in the PLGA matrix at (**A**) 75:25, (**B**) 50:50, (**C**) 25:75, and (**D**) 0:100 (PLGA:CNF [wt:wt]) at a PLGA density of 0.025 g/mL.

PLGA:CNF material properties

Conductivity

The results of this study also provided evidence that increasing the CNF weight ratio in PLGA increased conductivity, as shown in Figure 2. Conductivity increased as greater amounts of CNF were added to pure PLGA, from 0 $S \cdot m^{-1}$ for pure PLGA (100:0 wt%) to 5.5×10^{-3} $S \cdot m^{-1}$ for pure CNF (0:100 wt%), as compared with natural heart tissue (ranging from 0.16 $S \cdot m^{-1}$ longitudinally to 0.005 $S \cdot m^{-1}$transversely24). Clearly, the increased conductivity of the composites was due to the uniform distribution of more conductive CNF within the sample (Figure 1). Therefore, as anticipated, the addition of CNF increased conductivity.

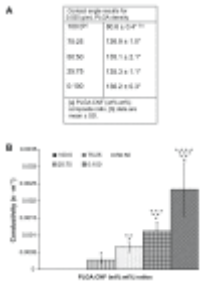

Figure 2

Material characteristics of PLGA:CNF (wt%:wt%) looking at (**A**) wettability of the material at different PLGA density ratios, indicating that all materials are hydrophobic. (**B**) Example of material conductivity at a PLGA density of 0.025 g/mL, providing **...**

Wettability

Contact angle experiments suggested that altering the PLGA density did not affect the wettability of the composite. For example, contact angle measurements for a 50:50 [PLGA:CNF (wt%:wt%)] sample ranged from 132.0° for a 0.1 g/mL PLGA density to 135.0° for a 0.0125 g/mL PLGA density. Contact angle measurements also suggested that adding CNF made the materials more hydrophobic, as compared with the pure PLGA samples (Figure 2A). For example, pure PLGA for all PLGA densities (0.1 g/mL, 0.05 g/mL, 0.025 g/mL, and 0.0125 g/mL) was 81.0° ± 1.0°, whereas the 75:25 [PLGA:CNF (wt%:wt%)] samples were 125° ± 3.0°. This is important because cardiovascular research, particularly with biomaterials and cardiomyocytes, has shown that when a material is more hydrophobic, protein adsorption will occur more readily than with more hydrophilic materials, and mediate cell attachment and spreading.25

Material degradation and pH readings

Results of the degradation study showed that the percentage weight loss from pure PLGA was the greatest among all the substrates tested (Figure 3A). As expected, no weight loss was observed on pure CNF samples. Specifically, for a PLGA density of 0.025 g/mL, the weight loss from 75:25 samples was 10% less that than from pure PLGA, whereas the 50:50 and 25:75

sample ratios [PLGA:CNF (wt%:wt%)] had a higher percent weight loss than from pure PLGA after 21 days of incubation. All sample ratios had 25% or more, which was less than from pure PLGA, at 28 days of incubation; and 30% or more, which was less than pure PLGA, after 36 days of incubation. This indicates that the dispersion status of CNF in PLGA played an important role in decreasing the degradation behavior of the study composites.

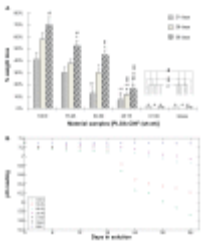

Figure 3

PLGA:CNF material characteristics. (**A**) Percentage weight loss for 100:0, 75:25, 50:50, 27:75, and 0:100 sample ratios (PLGA:CNF [wt%:wt%]) and an etched glass coverslip incubated in phosphate-buffered solution under standard incubation conditions. (**B ...**

The inhibitory effect of CNF on PLGA weight loss was more significant after longer incubation times, and correlated with the pH buffering effect of CNF. Specifically, the pH drop was less than 5% for all the composites during the first 21 days of incubation, but was approximately 10% for pure PLGA (Figure 3B). During days 22–36 of incubation, the pH drop for all the composites and PLGA was faster than during the first 3 weeks of incubation. For a PLGA density of 0.025 g/mL, the pH drop was 22% for pure PLGA, and was 15% for the 75:25 ratio [PLGA:CNF (wt%:wt%)], 8% for the 50:50 ratio [PLGA:CNF (wt%:wt%)], and only 5% for the 25:75 ratio [PLGA:CNF (wt%:wt%)] after 36 days of incubation. When PLGA degrades, it separates into lactic acid and glycolic acid, which in turn will increase the acidity of the surrounding medium. Therefore, higher pH readings were observed at higher CNF ratios as compared with pure PLGA samples, due to less PLGA degradation material in the medium.

Tensile tests

The results show that addition of CNF to the PLGA composite greatly enhanced the composite tensile strength (Figure 4). Specifically, the addition of 25% CNF (percent total weight) to pure PLGA increased the Young's modulus by over 2500%, while the addition of 50% CNF (percent total weight) increased the Young's modulus by about 3500% and the addition of 75% CNF (percent total weight) increased the Young's modulus by about 2100%. Compared with native cardiac heart tissue, the composites had mechanical properties that were stiffer than native heart muscle, which is made of collagen and is elastomeric with a stiffness of approximately 50–100 kPa during diastole.[26–29] However, the modulus of active myocardium during systole is approximately 20-fold higher,[30,31] so more closely resembles that of PLGA:CNF composites. These results indicated that the addition of CNF increased the composite tensile strength to

mirror better the ability to strengthen the myocardium. On the other hand, the addition of CNF to the PLGA composites decreased the percent elongation at material failure; 86% for the addition of 25% CNF (percent total weight) to 4% for the addition of 75% CNF (percent total weight), thus indicating an inverse relationship between the addition of CNF to PLGA and elongation at failure. This is not surprising given that the continual addition of CNF to a matrix will hinder the ability of PLGA to adhere to CNF and strengthen the material.

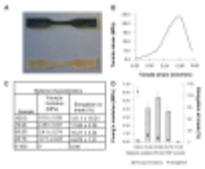

Figure 4

Addition of CNF to PLGA greatly increased the tensile strength and created a material with properties closer to those of normal human myocardium. (**A**) Photograph of prepared flat test samples. Dimensions of the sample were: gauge length 7.62 mm, width **...**

Atomic force microscopy and material topography

Increased topographical features were present throughout the atomic force microscopy results for all materials compared with an etched glass surface. It was shown that adding CNF to the PLGA solution increased the topographical features and also the surface area of the substrate (Figure 4). Specifically, pure PLGA had a 10% surface area increase compared with an etched glass cover slip of the same dimensions. With the addition of 25% CNF (wt%) to PLGA, the surface area increased by 45%. A 50% CNF (wt%) addition to PLGA increased the surface area by approximately 60%. With the addition of 75% CNF (wt%) to PLGA and 100% CNF, a lesser percent surface area increase was observed. Specifically, the addition of 75% CNF (wt%) to PLGA increased the surface area by about 28%, whereas 100% CNF increased the surface area by about 22%. This is mainly because when too many CNF are added to PLGA, significant agglomeration occurs, creating more micro features and fewer nano features, which actually decreases the surface area. Importantly, this indicates that the addition of nanomaterials to a system can increase topographical features, which in turn can increase cell attachment and growth.[32]

Protein adsorption

The results of this study indicated that addition of CNF to PLGA directly affects initial protein adsorption events. When normalized to pure PLGA samples, the OD reading data for both fibronectin and vitronectin, when compared with the atomic force microscopy surface area percent increase, showed significantly greater adsorption of vitronectin and fibronectin onto composites when adding CNF up to 50% (weight ratio), then a decrease when adding more CNF to the matrix (Figure 5C and D). These results indicate a direct correlation between surface

topography and protein adsorption. This is important because protein adsorption has been correlated with the wound healing process. For example, fibronectin is a known chemoattractant for several cell types which play a role in the wound healing process,[33] including fibroblasts, endothelial cells, and macrophages. In addition, fibronectin generates a scaffold to which other extracellular matrix components can attach. During the healing phase after a myocardial infarction, large amounts of plasma proteins, namely fibronectin, are deposited around the area of necrosis to promote cell attachment and growth[34,35] within one day of an infarct.

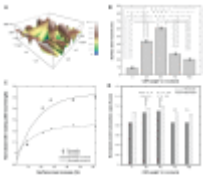

Figure 5

Addition of CNF to the PLGA substrate alters the topography of the material. Using an Asylum MFP three-dimensional atomic force microscope (scan rate 1.0 Hz, AC mode with 256 × 256 scan points and lines), (**A**) CNF are shown for a 25:75 ratio (PLGA:CNF **...**

Cardiomyocyte compatibility

For cardiomyocyte adhesion, results from this study showed that, after 4 hours of cell culture, the 0.05 mg/mL and 0.025 mg/mL PLGA densities with the 75:25 and 50:50 ratios [PLGA:CNF (wt%:wt%)] had the highest cardiomyocyte density. The results of the proliferation assay showed the same trend as that observed during the adhesion assay (Figure 6). Specifically, the 75:25 and 50:50 sample ratios [PLGA:CNF (wt%:wt%)] at PLGA densities of 0.05 mg/mL and 0.025 mg/mL had the highest cardiomyocyte densities, whereas the 100:0 sample ratio [PLGA:CNF (wt%:wt%)] for all PLGA densities had the lowest cardiomyocyte densities after 24, 72, and 120 hours. Due to the slower proliferation of the cardiomyocytes compared with other cells (around 72 hours for cell doubling times), one would not see a typical doubling time every 48 hours. Also, Live/Dead images showed an increase in cell density over time, with 60%–80% confluence by day 5 for all PLGA:CNF ratios (Figure 7).

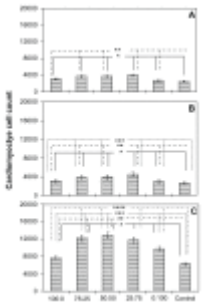

Figure 6

Cardiomyocyte cell proliferation on a PLGA density of 0.025 g/mL after (**A**) 24, (**B**) 72, and (**C**) 120 hours on 100 nm diameter PLGA:CNF composite materials of interest in this study.

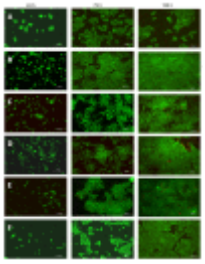

Figure 7

Live/Dead® assay images after 24, 72, and 120 hours on the various weight ratios (**A**) 100:0, (**B**) 75:25, (**C**) 50:50, (**D**) 25:75, (**E**) 0:100, and (**F**) glass with a PLGA density of 0.025 g/mL.

Furthermore, immunofluorescence staining of specific cardiac biomarkers (cardiac troponin T, connnexin-43, and α-SCA) was conducted in the present study (Figure 8), indicating normal cardiomyocyte activity for all materials. When using ImageJ software, cardiac biomarker staining followed the same patterns showed for all cardiomyocyte adhesion and proliferation experiments (Figure 6). Specifically, 50:50 [PLGA:CNF (wt%:wt%)] ratio samples had the highest staining area percentage (63% for cardiac troponin T, 60% for connexin-43, and 61% for α-SCA) for all cardiac biomarkers. Similarly, cells were observed to have elongated features at all PLGA:CNF ratios. There were no dissimilar morphological features observed among the different weight ratios.

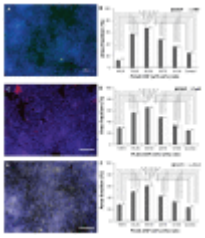

Figure 8

Immunofluorescence staining for cardiomyocyte biomarkers on a 0.025 g/mL PLGA density PLGA:CNF composite after 120 hours of incubation. (**A**) Cardiac troponin T (green) biomarker with DAPI stain (blue) on a 50:50 (PLGA:CNF [wt%:wt%]) sample. (**B**) Connexin-43**...**

Go to:

Discussion

Due to the importance of improved and safer approaches to coronary and intracranial revascularization, many materials, such as alginate[37] and polytetrafluoroethylene,[38] have been developed to promote cardiomyocyte function after a myocardial infarction. Research has shown that composite materials composed of different matrices can stabilize heart tissue to decrease the consequences of a myocardial infarction, and such approaches include but are not limited to culturing patient tissue,[39,40] direct cell injection,[41,42] and biomaterial scaffolds.[43,44] Recently, the advent of advanced novel nanobiomaterials with improved properties capable of being used

in several biomedical applications simultaneously has transformed the field of biomedical research and the world of cardiovascular biomaterials. One such example is the use of a PLGA material with CNF embedded to create a “patch” for an infarcted area of the heart. The present work addresses the underlying mechanism that alters the material-cell interaction on a novel material and sheds light on cardiomyocyte growth and function, which in turn will help develop alternative bioinspired systems for cardiovascular applications.

Specifically, the addition of CNF to a PLGA solution increased material tensile strength to mimic native heart tissue (approximately 0.5–2.00 MPa[30,31]) and increased cardiomyocyte growth. It was shown here that a PLGA density of 0.025 g/mL with 75:25 and 50:50 ratios (PLGA:CNF [wt%:wt%]) had the highest Young’s modulus, and could closely mimic native heart tissue. On the other hand, the 25:75 ratio (PLGA:CNF [(wt%:wt%]) was closer to the strength characteristics of native heart tissue, but the material had very limited elongation capability (about 2% at breaking point), and this is very important because native heart tissue is continuously expanding and contracting.

Additionally, adding CNF up to a specific weight ratio (50:50 [PLGA:CNF (wt%:wt%)]) increased the surface area, nanoscale roughness, and ultimately vitronectin and fibronectin adsorption capacity (Figure 5). In the past, researchers have found that the adsorption and bioactivity of vitronectin and fibronectin increases on nanophase ceramics and that this enhanced osteoblast function (adhesion, proliferation, and differentiation).[45] These studies reported that the roughness was closer to the nanometer roughness of bone in nanoceramics, leading to more bone growth on nanophase ceramics.[45] Even though the myocardium is made up of cardiac muscle, the research here suggests that increasing the nanoroughness of a biomaterial will promote the growth of cardiac-specific muscle, which is parallel to the nanoroughness and increases potential vascular smooth muscle cell and endothelial cell growth.[46]

Clearly, CNF possess nanoscale geometries which imitate the extracellular matrix of various tissues (such as the heart), leading to improved cytocompatibility of these materials. This correlates directly with the topography of PLGA:CNF composites which can control protein adsorption events via changes in surface energy (Figure 5C and D). Importantly, it is also known that a material can be too rough and can hinder cellular activity.[32] For example, Yang et al used diamond films with nanometer and micron scale topographies fabricated by microwave plasma-enhanced chemical vapor deposition and hydrogen plasma treatment, and showed that microsized diamond topographies decreased osteoblast cell adhesion and proliferation compared with nanosized diamond topographies.[32]

In addition, we were able to show that when adding CNF to PLGA, the composite became conductive, whereas the PLGA matrix alone was not conductive. The conductivity values measured in the present work were lower than that of heart tissue (ranging from 0.16 $S \cdot m^{-1}$ longitudinally to 0.005 $S \cdot m^{-1}$transversely),[24] but future techniques (such as CNF

alignment) may increase anisotropic conductivity[47] to match that of heart tissue. Pedrotty et al[48] showed that numerous cardiac cell functions (including adhesion, proliferation, and migration) may be modulated by electrical stimulation, hence required the use of a conductive material in cardiac applications. Mihardja et al[49] also demonstrated that enhanced myocardial repair following an ischemic injury could be achieved using conductive polymers, such as polypyrrole. The increasing conductivity of a material with greater CNF ratios has the potential to propagate electrical signals from contraction of native heart tissue to reduce arrhythmias. Additionally, cell experiments showed the expression of cardiac differentiation markers (cardiac troponin T, connexin-43, and α-SMA) as confirmed by fluorescence microscopy, thus indicating normal cardiomyocyte function.

Interestingly, when combining protein adsorption capacity, surface area percent increases, and tensile testing, all results point to either the 75:25 or a 50:50 material ratio (PLGA:CNF [wt%:wt%]) as the best composites for cardiomyocyte growth, which correlates with previous published results.[15] This research provides the first evidence that addition of CNF to PLGA can increase nanosurface roughness, which increases material surface area without altering wettability, to increase vitronectin and fibronectin adsorption capacity, while at the same time generating tensile strength that closely resembles that of native heart tissue, ultimately to alter the interactions between the materials and cardiomyocytes (Figure 9).

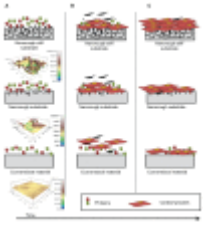

Figure 9

Schematic illustration, with a three-dimensional atomic force microscopy topographical image (scan rate 1.0 Hz, AC mode with a 256 × 256 scan points and lines), of the proposed mechanism by which PLGA:CNF materials may be superior to conventional **...**

When considering our cardiopatch material applications, future in vivo work must look at CNF compatibility after PLGA degradation. Once the cardiopatch is sutured into place,[50–52] PLGA will begin to degrade and CNF exposure will increase and become embedded into its host, because CNF are nonbiodegradable. In vitro experiments have revealed that cell-matrix interactions limit cell motility, growth, and full scaffold colonization,[53,54] and therefore scaffold degradation is highly desirable to allow for cell replacement. Also, research has shown that carbon-based nanotubes and fibers are biocompatible platforms for neuronal growth and cell differentiation.[55,56] Therefore, our material has the potential to exploit both of these desirable traits in a tissue engineering matrix, ie, PLGA degradation to allow for better cell growth and CNF for cell progress and continual development.

Go to:

Conclusion

This present work demonstrates a few underlying mechanisms to elucidate the way in which cardiomyocytes grow on PLGA and CNF composites. As the CNF weight to specific ratios (50:50 was increased [PLGA:CNF (wt%:wt%)]), this study found that nanoscale roughness increases to promote vitronectin and fibronectin adsorption and ultimately increase cardiomyocyte growth, as well as increasing tensile and conductivity properties. Additionally, it was determined that a PLGA density of 0.025 g/mL at a 50:50 (PLGA:CNF [wt%:wt%]) ratio caused the highest cardiomyocyte growth, indicating that the PLGA density can alter cardiomyocyte adhesion and proliferation to a certain degree. Scanning electron micrographs showed uniform CNF dispersion within the PLGA matrix and a close interaction between cardiomyocytes and substrates, while contact angle experiments suggested that changes in wettability did not occur, thus demonstrating that a simple solution-mixing-drying-based synthesis route can be adopted to develop PLGA:CNF hybrid biocomposites over a broad composition range, possessing a uniform distribution of CNF without any clustering. In summary, cardiomyocyte growth on PLGA:CNF composites was enhanced by creating nanotopographical features due to the addition of CNFs which, in turn, increased protein adsorption capacitance, creating a composite which closely resembles native heart tissue.

Go to:

Acknowledgments

The authors would like to thank the National Science Foundation Graduate Research Fellowship Program (1058262), the National Science Foundation (DMR-0805172), the Hermann Foundation, and the Leadership Alliance Summer Research Early Identification Program (SR-IEP) for funding and support. The authors would also like to thank Lei Yang (for assistance with analysis of atomic force microscopy data), Jiangdong Deng and Jason Tresback (Harvard University, for assistance with atomic force microscopy), Urlike Mende (for assistance with cardiomyocyte experiments), Geoff Williams (Brown University Leduc Center, for assistance with fluorescence microscopy), and Paul Waltz (Brown University Price Laboratories, for tensile testing). This work was partially performed at the Center for Nanoscale Systems, a member of the National Nanotechnology Infrastructure Network, which is supported by the National Science Foundation (ECS-0335765).

Go to:

Footnotes

Disclosure

The authors report no conflicts of interest in this work.

Go to:

References

1. Alpert JS, Thygesen K. A call for universal definitions in cardiovascular disease. Circulation.2006;114(8):757–758. [PubMed]

2. Maton A. Human Biology and Health. Englewood Cliffs, NJ: Prentice Hall; 1993.

3. Lloyd-Jones D, Adams RJ, Brown TM, et al. Executive Summary: Heart Disease and Stroke Statistics – 2010 Update. Circulation. 2010;121(7):948–954. [PubMed]

4. Björn D. Cardiovascular disease risk factors: epidemiology and risk assessment. Am J Cardiol.2010;105(Suppl 1):3A–9A. [PubMed]

5. Dzau VJ, Antman EM, Black HR, et al. The cardiovascular disease continuum validated: clinical evidence of improved patient outcomes. Circulation. 2006;114(25):2850–2870. [PubMed]

6. Germani A, Di Rocco G, Limana F, Martelli F, Capogrossi MC. Molecular mechanisms of cardiomyocyte regeneration and therapeutic outlook. Trends Mol Med. 2007;13(3):125–133. [PubMed]

7. Laflamme MA, Murry CE. Regenerating the heart. Nat Biotechnol. 2005;23(7):845–856. [PubMed]

8. Cohen S. Rebuilding broken hearts. Sci Am. 2004;291(5):44. [PubMed]

9. Vunjak-Novakovic G, Tandon N, Godier A, et al. Challenges in cardiac tissue engineering. Tissue Eng Part B Rev. 2009;16(2):169–187. [PMC free article] [PubMed]

10. Saw SH, Wang K, Yong T, Ramakrishna S. Nanotechnologies for the Life Sciences. Weinheim, Germany: Wiley-VCH Verlag GmbH and C, KGaA; 2007. Polymeric nanofibers in tissue engineering.

11. Cappelletti M, Muggleton N, Walsh V. Quantity without numbers and numbers without quantity in the parietal cortex. Neuroimage. 2009;46(2):522–529. [PMC free article] [PubMed]

12. Shuangyin W, Noel K, Sanping J, Xin W. Controlled synthesis of dendritic Au@Pt core-shell nanomaterials for use as an effective fuel cell electrocatalyst. Nanotechnology. 2009;20(2):025605. [PubMed]

13. Mu Y, Liang H, Hu J, Jiang L, Wan L. Controllable Pt nanoparticle deposition on carbon nanotubes as an anode catalyst for direct methanol fuel cells. J Phys Chem B. 2005;109(47):22212–22216. [PubMed]

14. Dvir T, Timko BP, Brigham MD, et al. Nanowired three-dimensional cardiac patches. Nat Nanotechnol.2011;6(11):720–725. [PMC free article] [PubMed]

15. Stout DA, Basu B, Webster TJ. Poly(lactic-co-glycolic acid): carbon nanofiber composites for myocardial tissue engineering applications. Acta Biomater. 2011;7(8):3101–3112. [PubMed]

16. Komarneni S. Nanocomposites. J Mater Chem. 1992;2(12):1219–1230.

17. Chantidis CA. Nanomechanical and nanotribological properties of carbon-based thin films: a review.International Journal of Refractory Metals and Hard Materials. 2010;28(1):51–70.

18. Liu H, Webster TJ. Nanomedicine for implants: a review of studies and necessary experimental tools.Biomaterials. 2007;28(2):354–369. [PubMed]

19. Verma A, Stellacci F. Effect of surface properties on nanoparticle-cell interactions. Small. 2010;6(1):12–21. [PubMed]

20. American Society for Testing and Materials. Standard Test Method for Tensile Properties of Plastics.D638-610. West Conshohocken, PA: American Society for Testing and Materials; 2010.

21. Zheng H-X, Liu S-S, Tian W-M, Yan H-J, Zhang Y, Li Y. A three-dimensional in vitro culture model for primary neonatal rat ventricular myocytes. Current Applied Physics. 2012;12(3):826–833.

22. Tribulova N, Shneyvays V, Mamedova L, et al. Enhanced connexin-43 and α-sarcomeric actin expression in cultured heart myocytes exposed to triiodo-l-thyronine. J Mol Histol. 2004;35(5):463–470.[PubMed]

23. Carrier L, Boheler K, Chassagne C, et al. Expression of the sarcomeric actin isogenes in the rat heart with development and senescence. Circ Res. 1992;70(5):999–1005. [PubMed]

24. Roberts-Thomson KC, Kistler PM, Sanders P, et al. Fractionated atrial electrograms during sinus rhythm: relationship to age, voltage, and conduction velocity. Heart Rhythm. 2009;6(5):587–591. [PubMed]

25. Christman KL, Lee RJ. Biomaterials for the treatment of myocardial infarction. J Am Coll Cardiol.2006;48(5):907–913. [PubMed]

26. Engelmayr GC, Cheng M, Bettinger CJ, Borenstein JT, Langer R, Freed LE. Accordion-like honeycombs for tissue engineering of cardiac anisotropy. Nat Mater. 2008;7(12):1003–1010.[PMC free article] [PubMed]

27. Jalil J, Doering C, Janicki J, Pick R, Shroff S, Weber K. Fibrillar collagen and myocardial stiffness in the intact hypertrophied rat left ventricle. Circ Res. 1989;64(6):1041–1050. [PubMed]

28. Mirsky I, Parmley WW. Assessment of passive elastic stiffness for isolated heart muscle and the intact heart. Circ Res. 1973;33(2):233–243. [PubMed]

29. Boublik J, Park H, Radisic M, et al. Mechanical properties and remodeling of hybrid cardiac constructs made from heart cells, fibrin, and biodegradable, elastomeric knitted fabric. Tissue Eng. 2005;11(7–8):1122–1132. [PubMed]

30. Phillips CA, Petrofsky JS. Myocardial material mechanics: characteristic variation of the circumferential and longitudinal systolic moduli in left ventricular dysfunction. J Biomech. 1984;17(8):561–568. [PubMed]

31. Westerhof N, Stergiopulos N, Noble MIM. Snapshots of Hemodynamics: An Aid for Clinical Research and Graduate Education. New York, NY: Springer; 2010.

32. Yang L, Sheldon BW, Webster TJ. The impact of diamond nanocrystallinity on osteoblast functions.Biomaterials. 2009;30(20):3458–3465. [PubMed]

33. Grinnell F. Fibronectin and wound healing. J Cell Biochem. 1984;26(2):107–116. [PubMed]

34. Kent SP. Diffusion of plasma proteins into cells – a manifestation of cell injury in human myocardial ischemia. Am J Pathol. 1967;50(4):623–637. [PMC free article] [PubMed]

35. Casscells W, Kimura H, Sanchez JA, Yu ZX, Ferrans VJ. Immunohistochemical study of fibronectin in experimental myocardial infarction. Am J Pathol. 1990;137(4):801–810. [PMC free article] [PubMed]

36. Willems IE, Arends JW, Daemen MJ. Tenascin and fibronectin expression in healing human myocardial scars. J Pathol. 1996;179(3):321–325. [PubMed]

37. Landa N, Miller L, Feinberg MS, et al. Effect of injectable alginate implant on cardiac remodeling and function after recent and old infarcts in rat. Circulation. 2008;117(11):1388–1396. [PubMed]

38. Krupnick AS, Kreisel D, Engels FH, et al. A novel small animal model of left ventricular tissue engineering. J Heart Lung Transplant. 2002;21(2):233–243. [PubMed]

39. Wei H-J, Chen C-H, Lee W-Y, et al. Bioengineered cardiac patch constructed from multilayered mesenchymal stem cells for myocardial repair. Biomaterials. 2008;29(26):3547–3556. [PubMed]

40. Ramaswamy S, Gottlieb D, Engelmayr GC, Jr, et al. The role of organ level conditioning on the promotion of engineered heart valve tissue development in vitro using mesenchymal stem cells. Biomaterials.2010;31(6):1114–1125. [PMC free article] [PubMed]

41. Perin EC, Dohmann HF, Borejevic R, et al. Time course of improvement following stem cell injections in humans with heart failure. J Am Coll Cardiol. 2004;43(5):A187.

42. Shintani Y, Fukushima S, Varela-Carver A, et al. Donor cell-type specific paracrine effects of cell transplantation for post-infarction heart failure. J Mol Cell Cardiol. 2009;47(2):288–295. [PubMed]

43. Callegari A, Bollini S, Iop L, et al. Neovascularization induced by porous collagen scaffold implanted on intact and cryoinjured rat hearts. Biomaterials. 2007;28(36):5449–5461. [PubMed]

44. Siepe M, Giraud M-N, Pavlovic M, et al. Myoblast-seeded biodegradable scaffolds to prevent post-myocardial infarction evolution toward heart failure. J Thorac Cardiovasc Surg. 2006;132(1):124–131.[PubMed]

45. Webster TJ, Ergun C, Doremus RH, Siegel RW, Bizios R. Specific proteins mediate enhanced osteoblast adhesion on nanophase ceramics. J Biomed Mater Res. 2000;51(3):475–483. [PubMed]

46. Miller DC, Thapa A, Haberstroh KM, Webster TJ. Endothelial and vascular smooth muscle cell function on poly(lactic-co-glycolic acid) with nano-structured surface features. Biomaterials. 2004;25(1):53–61.[PubMed]

47. Bal S. Experimental study of mechanical and electrical properties of carbon nanofiber/epoxy composites.Mater Des. 2010;31(5):2406–2413.

48. Pedrotty DM, Koh J, Davis BH, Taylor DA, Wolf P, Niklason LE. Engineering skeletal myoblasts: roles of three-dimensional culture and electrical stimulation. Am J Physiol Heart Circ Physiol.2005;288(4):H1620–H1626. [PubMed]

49. Mihardja SS, Sievers RE, Lee RJ. The effect of polypyrrole on arteriogenesis in an acute rat infarct model. Biomaterials. 2008;29(31):4205–4210. [PMC free article] [PubMed]

50. Nicolosi A, Weng Z, Detwiler P, Spotnitz H. Simulated left ventricular aneurysm and aneurysm repair in swine. J Thorac Cardiovasc Surg. 1990;100(5):745–755. [PubMed]

51. Sakamoto Y, Mizuno A, Buckberg GD, Baretti R, Child JS, Fonarrow G. Restoring the remodeled enlarged left ventricle: experimental benefits of in vivo porcine cardioreduction in the beating open heart. J Cardiac Surg. 1998;13(6):429–439. [PubMed]

52. Cui J, Li J, Mathison M, et al. A clinically relevant large-animal model for evaluation of tissue-engineered cardiac surgical patch materials. Cardiovasc Revasc Med. 2005;6(3):113–120. [PubMed]

53. Lutolf MP, Hubbell JA. Synthetic biomaterials as instructive extracellular microenvironments for morphogenesis in tissue engineering. Nat Biotechnol. 2005;23(1):47–55. [PubMed]

54. Hollister SJ. Porous scaffold design for tissue engineering. Nat Mater. 2005;4(7):518–524. [PubMed]

55. Mattson M, Haddon R, Rao A. Molecular functionalization of carbon nanotubes and use as substrates for neuronal growth. J Mol Neurosci. 2000;14(3):175–182. [PubMed]

56. Hu H, Ni Y, Montana V, Haddon RC, Parpura V. Chemically functionalized carbon nanotubes as substrates for neuronal growth. Nano Lett. 2004;4(3):507–511. [PMC free article] [PubMed]